



Soft Matter

Design Rules for 2D Field Mediated Assembly of Different Shaped Colloids into Diverse Microstructures

Journal:	<i>Soft Matter</i>
Manuscript ID	SM-ART-08-2022-001078.R2
Article Type:	Paper
Date Submitted by the Author:	20-Nov-2022
Complete List of Authors:	Hendley, Rachel; Johns Hopkins University Zhang, Lechuan; Johns Hopkins University Bevan, Michael; Johns Hopkins University

SCHOLARONE™
Manuscripts

Design Rules for 2D Field Mediated Assembly of Different Shaped Colloids into Diverse Microstructures

*Rachel S. Hendley, Lechuan Zhang, Michael A. Bevan**

Chemical & Biomolecular Engineering, Johns Hopkins University, Baltimore, MD 21218

Abstract

Assembling different shaped particles into ordered microstructures is an open challenge in creating multifunctional particle-based materials and devices. Here, we report the two-dimensional (2D) AC electric field mediated assembly of different shaped colloidal particles into amorphous, liquid crystalline, and crystalline microstructures. Particles shapes investigated include disks, ellipses, squares, and rectangles, which show how systematic variations in anisotropy and corner curvature determine the number and types of resulting microstructures. AC electric fields induce dipolar interactions to control particle positional and orientational order. Microstructural states are determined via particle tracking to compute order parameters, which agree with computer simulations and show how particle packing and dipolar interactions together produce each structure. Results demonstrate how choice of particle shape and field conditions enable kinetically viable routes to assemble nematic, tetratic, and smectic liquid crystal structures as well as crystals with stretched 4- and 6- fold symmetry. Results show it is possible to assemble all corresponding hard particle phases, but also show how dipolar interactions influence and produce additional microstructures. Our findings provide design rules for the assembly of diverse microstructures of different shaped particles in AC electric fields, which could enable scalable and reconfigurable particle-based materials, displays, and printing technologies.

keywords: anisotropic particles, liquid crystals, crystals, superellipses, AC electric fields

Introduction

Designing, controlling, and optimizing methods to assemble diverse microstructures of different shaped particles could enable numerous particle-based materials and devices with novel properties.¹ As natural inspiration, many plant and animal tissues with periodic structures of non-spherical repeat units exhibit exceptional unique multifunctional properties (*e.g.*, mechanical, optical, adhesive, wetting, acoustic, etc.^{2,3}). From another perspective, metasurfaces^{4,5} consisting of 2D ordered configurations of non-spherical repeat units also display unprecedented electromagnetic functionalities (*e.g.*, beam steering, shaping, cloaking, etc.) without natural analogs. In relation to these examples, some biological material functionalities have been recapitulated in synthetic materials using microfabrication, and metasurface properties have also been demonstrated on small scales via microfabrication. However, assembling different shaped colloids on surfaces could provide an alternate route to capturing key structural features for scalable large area coatings and reconfigurable metadevices.⁶

Different shaped particles can form a variety of 2D amorphous, liquid crystal, plastic crystal, and crystal microstructures – in contrast to only amorphous or simple crystal states for spheres or disks. Shape differences involving aspect ratio and corner curvature alter the number and symmetry of microstructures in hard particle systems via packing effects (entropy).⁷ As an

* To whom correspondence should be addressed: mavevan@jhu.edu

example of varying aspect ratio, hard ellipses yield plastic crystals (positional order only) or nematic liquid crystals (orientational order only) depending on their aspect ratio, which occur intermediate to liquid and 6-fold crystal states.⁸ To illustrate effects of particle corners, the number of corners on 2D hard polygons⁹ or curvature of rounded hard square corners¹⁰ change symmetry in crystal, plastic crystal, and “*x*-atic” states (where *x*=tri-, tetra-, hexa-) intermediate to liquid and crystal states. Although realistic soft attractive, repulsive, and directional potentials between different shaped particles can alter microstructures compared to hard particles,¹¹ these prior studies reveal the microstructural diversity that can be obtained with different shaped particles.

Despite the promise for realizing diverse microstructured materials from different shaped colloidal building blocks,^{12,13} success has been limited in creating ordered structures from micron scale colloidal particles (*e.g.*, ~0.1-10 μm). This length scale range encompasses important wavelengths of the electromagnetic spectrum,² and also corresponds to many other biological ordered microstructures with emergent properties of interest.³ To illustrate limitations to assembling ordered microstructures, amorphous glassy configurations are often the default state that results from concentrating anisotropic colloids into monolayers.^{14,15} It is perhaps likely that the additional degrees of freedom in particle shape that yield microstructural variability due to positional and orientational order also contribute to complex assembly pathways leading to disordered metastable and arrested states.

Using electric fields to induce particle dipoles has been perhaps the most promising approach to date for assembling ordered states of different shaped colloids. Examples include nematic structures of ellipsoids,¹⁶ smectic¹⁷ and plastic crystal¹⁸ structures of rods, and crystalline states of dumbbells,¹⁹ ellipsoids,²⁰ and nanowires.²¹ However, even though such states have been observed for specific particle shapes in electric fields, the general design rules are unknown for obtaining desired microstructures based on choosing particle shape and field properties. Practically, understanding the relationship between particle shape, applied field amplitude and frequency, and final microstructure is non-trivial due to the complex interplay of field mediated dipolar interactions²²⁻²⁴ and entropy mediated packing.⁷ In addition, kinetically viable routes to obtain significant order in experiments is often limited by an abundance of potential defective states including differently ordered sub-domains and particle shape dependent topological defects.

Here, we report a general method using nonuniform AC electric fields to systematically assemble a variety of photolithographic epoxy particle shapes into diverse microstructures with different positional and orientational order and local symmetries (**Fig. 1**). Practically, we investigate rapid, kinetically viable routes to assemble different particle shapes, with varying aspect ratio and corner curvature, into as many as possible target liquid crystal and crystalline microstructures. We show how field conditions and particle shape together can be designed to yield microstructures with minimal defects, including: amorphous, nematic, tetratic, smectic, and crystalline states with either isotropic or stretched 4-fold or 6-fold symmetry. We investigate superellipse prism particles that encompass a broad variety of particle shapes and allow continuous adjustment of particle shapes in terms of aspect ratio (*e.g.*, disks \rightarrow ellipses, squares \rightarrow rectangles) and corner curvature (*e.g.*, disks \rightarrow squares, ellipses \rightarrow rectangles). We show how microstructures depend on particle shape dependent packing and dipolar interactions in nonuniform fields that control transport, position, orientation, and concentration.²²⁻²⁴ Our systematic investigation of particle shape, including aspect ratio and corner curvature, reveals general design rules for obtaining desired microstructures based on choosing particle shape and field properties.

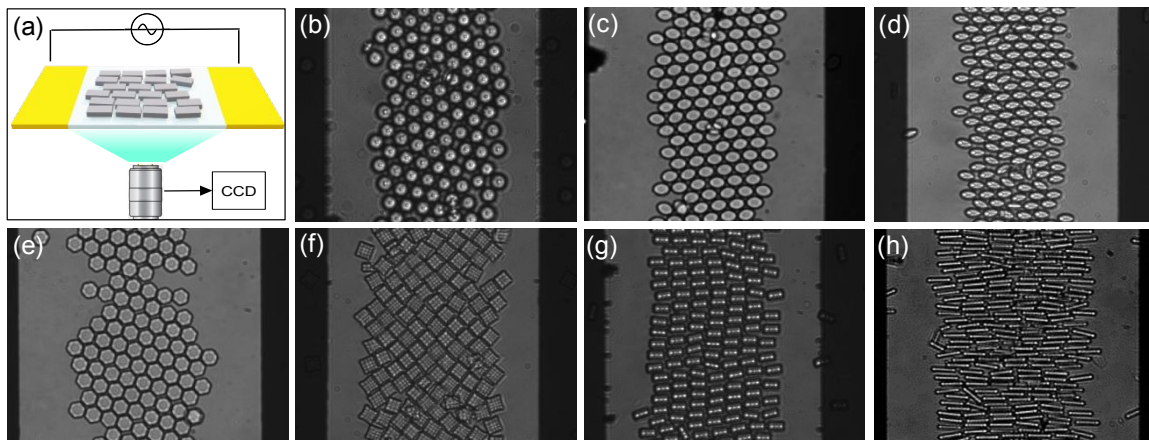


Fig. 1. 2D assembly of different shaped SU8 epoxy colloidal particles into ordered microstructures. (a) Microscopy images obtained for assembly between coplanar parallel electrodes in a 5MHz AC electric field for each shape, (radial size): (b) disks ($4.0\mu\text{m}$), (c) ellipses ($4.1\times 3.1\mu\text{m}$), (d) ellipses ($4.1\times 2.3\mu\text{m}$), (e) hexagons ($4.2\mu\text{m}$), (f) squares ($3.9\mu\text{m}$), (g) rectangles ($4.1\times 2.2\mu\text{m}$), and (h) rectangles ($5.1\times 1.2\mu\text{m}$). Electrode spacing is $100\mu\text{m}$ with applied field amplitudes ranging between $10\text{--}25\text{ V/mm}$. All particles are $1.7\mu\text{m}$ thick from profilometry. Cited particle dimensions serve as internal image scale bars.

Materials & Methods

Particle Fabrication. Superelliptical prism epoxy particles (**Fig. 1**) were fabricated using photolithography based on literature methods²⁵ adapted for particles with suitable charge for use in AC electric fields.^{22,24} In brief, Omnicoat (MicroChem) and SU-8 2002 (MicroChem) were sequentially spin coated on a silicon wafer. A photomask was used to pattern particles under a UV exposure energy of 80 mJ/cm^2 . Particles were removed from the substrate with Remover PG (MicroChem), then rinsed with isopropyl alcohol and dispersed in deionized water. Particles were washed with sulfuric acid to increase surface charge to prevent aggregation and deposition and produce enhanced induced dipoles in AC electric fields.^{22,24}

Microscopy & Particle Tracking. The optical microscopy cell is similar to previous studies.²⁶ An O-ring (McMaster-Carr) is placed on interdigitated gold electrodes ($300\mu\text{m}$ wide electrodes with a $100\mu\text{m}$ gap) on a glass slide. The particle dispersion is pipetted into the O-ring, which is then sealed with a cover slip to prevent evaporation. Wires are attached to the electrodes and an AC function generator (Agilent 33220A). Particles were imaged in an inverted microscope (Zeiss) with a $40\times$ objective. Videos were captured at 5 frames/s using a CCD camera (Hamamatsu, Orca-ER) and Streampix (Norpix) software. Particle position (x,y) and orientation (θ) were tracked using an algorithm in MATLAB that records centroid coordinates and long-axis orientation.²²

Monte Carlo Simulations. Monte Carlo simulations of superelliptical prism particles were performed in the canonical (NVT) ensemble using the methods and potentials in our previous work.²⁴ In brief, the energy, u_i , of each particle i is,

$$u_i = u_i^{df}(x_i, \theta_i) + \sum_{j=1, i \neq j}^{N_b} \left[u_{ij}^{dd}(x_i, \theta_i, \theta_j, x_{ij}, y_{ij}) + u_{ij}^{hp}(x_i, \theta_i, \theta_j, x_{ij}, y_{ij}) \right] \quad (1)$$

where x_i, y_i, θ_i are each particle's lab position and orientation coordinates, and $x_{ij}, y_{ij}, \theta_{ij}$ are relative particle position and orientation coordinates, and the exact functional forms for dipole-field, u^{df} , and dipole-dipole, u^{dd} , potentials for superelliptical prisms are described in detail in our previous

work.²⁴ Particles were constrained in 2D with periodic boundary conditions perpendicular to the electrodes. Particle geometry for the hard overlap condition⁷ is given by the superellipse equation, and particle volume was computed from the superellipse area times the prism thickness. More information about particle and medium properties used in the Clausius-Mossotti factor and the electric field are described in detail in our previous work.²⁴ Simulations were initialized from experimental particle positions. Experiments and simulations were matched by specifying the aspect ratio dependent stretched point dipole form²⁴ and then adjusting a concentration dependent amplitude correction^{24,27-29} to the dipolar potentials in Eq. (1) until differences between average experimental and simulated order parameters was minimized and equilibrated for 500,000 steps.

Order Parameters. Order parameters computed from particle coordinates were used to quantify microstructure in microscopy images and computer simulation renderings. Details of computing each parameter are described in detail in our prior work on hard superellipse phases.⁷ We briefly summarize calculations of order parameters. Global nematic order was characterized by the maximum average particle orientational order relative to a director, θ_2 , as,^{30,31}

$$S_2 = \max_{\theta_2} \langle \cos(2(\theta_i - \theta_2)) \rangle \quad (2)$$

and, global tetratic order was quantified by the maximum average relative orientation to a bidirector, θ_4 , as,^{32,33}

$$T_4 = \max_{\theta_4} \langle \cos(4(\theta_i - \theta_4)) \rangle \quad (3)$$

and global smectic order characterized by positional order with layering period, d , along the nematic director is given by,³⁴

$$\sigma = \max_d \langle \cos(2\pi r_{\theta_2}/d)(2 \cos \theta_2 - 1) \rangle \quad (4)$$

where positions, r_{θ_2} , are measured for each particle along the nematic director. To quantify crystallinity, we characterized average four- ($\langle C_4 \rangle$) or six- ($\langle C_6 \rangle$) fold connectivity by averaging each particle's local value as,³⁵

$$C_{n,i} = \frac{1}{n} \sum_{j=1}^{N_{b,i}} \begin{bmatrix} 1 & \chi_n^{ij} \geq 0.32 \\ 0 & \chi_n^{ij} < 0.32 \end{bmatrix}, \quad \chi_n^{ij} = \frac{|\text{Re}[\psi_{n,i} \psi_{n,j}^*]|}{|\psi_{n,i} \psi_{n,j}^*|} \quad (5)$$

where the local stretched bond orientational order parameter, $\psi_{n,i}$ (and its complex conjugate, $\psi_{n,i}^*$), was recently defined in our prior work as,⁷

$$\psi_{n,j} = \frac{1}{N_{b,j}} \left| \sum_{k=1}^{N_{b,j}} \exp(in\theta_{jk}) \right| = \frac{1}{N_{b,j}} \left| \sum_{k=1}^{N_{b,j}} \cos(n\theta_{jk}) + i \sin(n\theta_{jk}) \right| \quad (6)$$

where $N_{b,j}$ is the number of neighbors with bonds to particle j , and θ_{jk} is the angle between particle centers relative to an arbitrary axis. **Table 1** summarizes values of order parameters for assigning microstructures. Because the present study focuses on small system sizes with non-uniform density profiles in non-uniform external fields, we do not consider the long-range power-law decay of orientational order correlation functions, which is used to determine phase behavior in homogeneous large systems sizes.⁷

Table 1. Simplified order parameter based criteria for state determination (based on rigorous criteria for phase determination in large system size simulation results for homogeneous 2D superellipses⁷).

shape state	disk (Fig. 2)	ellipse (fig. 3)	square (Fig. 4)	rectangle (Fig. 5)
liquid	$\langle C_6 \rangle < 0.8$	$S_2 < 0.5$	$T_4 < 0.5$	$S_2 < 0.5$
nematic	-	$S_2 > 0.5$	-	$S_2 > 0.5$
tetratic	-	-	$T_4 > 0.5$	$T_4 > 0.5$
smectic	-	-	-	$\sigma > 0.5$
crystal (squ.)	-	-	$\langle C_4 \rangle > 0.8$	$\langle C_4 \rangle > 0.8$
crystal (hex.)	$\langle C_6 \rangle > 0.8$	$\langle C_6 \rangle > 0.8$	-	-

Results & Discussion

Overview of Approach

We use optical microscopy to observe quasi-2D assembly of different microfabricated SU8 epoxy particle shapes sedimented onto a microscope slide between coplanar parallel electrodes (**Fig. 1**). The particles are levitated within a quasi-2D layer above the glass surface by a balance of electrostatic repulsion and gravity so that the largest flat face of each “prism” particle is parallel to the substrate (with minimal out of plane Brownian rotation).³⁶ With application of MHz AC electric fields, particles have induced dipoles (via polarization of electrostatic double layers) and find their energy minimum position at the nonuniform electric field minimum (electrode gap center).^{22,23} Induced dipoles on particles also yield dipolar pair interactions that favor alignment of particles into chains along each particle’s long axis and alignment with the field direction. Dipolar interactions also generate repulsion between particles orthogonal to the field direction.^{24,27-29} Particles confined in nonuniform electric fields produce unique microstructures by minimizing their free energy, based on their potential energy determined by shape dependent dipolar interactions²⁴ and their configurational entropy determined by shape dependent packing effects.⁷

To simplify the description of the field’s action on the particles, it both concentrates anisotropic particles at the field minimum and aligns particles with the field. The field concentrates particles against their osmotic pressure,³⁷⁻³⁹ where higher field amplitudes compresses particles more strongly into crystals like those in **Fig 1**, and lower field amplitudes produce less compression to yield less condensed liquid and liquid-crystal states. Because the electric field is non-uniform, the concentration profile and microstructure display small spatial variations with higher concentrations/order obtained at the electrode central region and lower concentrations/order away from the central region. As a result, it is necessary to choose the correct field amplitude to produce the desired compression and microstructure. The AC field frequency also determines particle alignment relative to the field direction,^{22,23} so the field frequency can be chosen to optimize particle alignment prior to compression into highly ordered condensed liquid crystalline and crystalline states (and avoid glassy disordered condensed states^{15,40}).

The crystalline states in **Fig. 1** show different microstructures that are obtained for each shape after ~30 minutes of compression by the AC electric field. Each configuration is crystalline with significant local and global positional and orientational order. Simple observation (without image analysis) reveals the microstructures in **Fig. 1** depend on particle shape, where: (b, e) disks and hexagons generate crystals with six-fold hexagonal symmetry, (c, d) ellipses also pack with

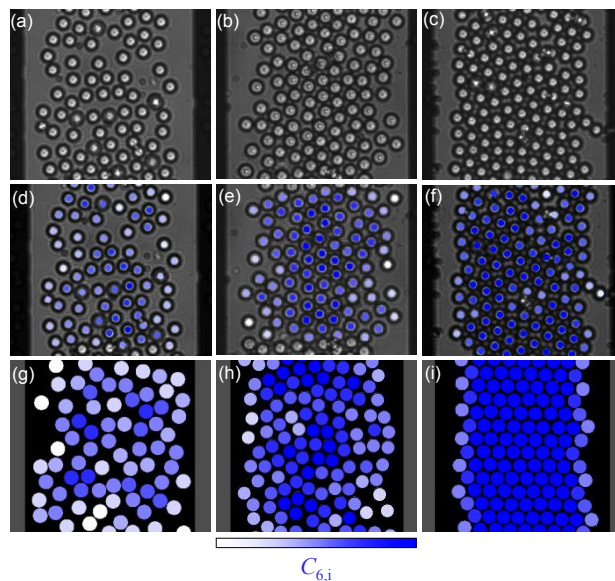


Fig. 2. Circular prisms (disks) with $r_x = 4.0\mu\text{m}$ in varying density liquid and crystalline states. Experiments without (a-c) and with (d-f) order parameter coloring and simulations (g-i) show assembled states as a function of average area fraction ($\langle\eta\rangle$), applied electric field amplitude (E_0), and local 6-fold connectivity ($C_{6,i}$, Eq. (5)). Particles are individually colored by $C_{6,i}$ from 0-1 (white-blue scale). Images and renderings show (left-to-right, “e” and “s” subscripts refer to experimental and simulated values) moderate density liquid ($\langle\eta\rangle=0.55$, $E_0=1\text{V/mm}$, $\langle C_{6,e}\rangle=0.52\pm 0.24$, $\langle C_{6,s}\rangle=0.42\pm 0.03$), high density liquid periphery coexisting with crystalline interior ($\langle\eta\rangle=0.67$, $E_0=2\text{V/mm}$, $\langle C_{6,e}\rangle=0.65\pm 0.27$, $\langle C_{6,s}\rangle=0.65\pm 0.02$), and crystalline state ($\langle\eta\rangle=0.8$, $E_0=10\text{V/mm}$, $\langle C_{6,e}\rangle=0.79\pm 0.24$, $\langle C_{6,s}\rangle=0.88\pm 0.00$). The AC electric field frequency in all cases is 5MHz.

six neighbors but with stretched six-fold symmetry as well as orientational order, (f) squares produce crystals with four-fold square symmetry, and (g, h) rectangles generate crystals with four-fold stretched symmetry. These results demonstrate how particle shape and dipolar interactions together control particle packing and orientation in crystal states. In the following, we systematically present and discuss in more detail for each particle shape how particle packing and applied field together affect local concentration, positional and orientational order, and the resulting microstructures.

Circular Prisms (Disks)

Experiments on disk particles (circular prisms) vs. field strength and concentration (**Fig. 2**) produce different microstructures based on their compression in the field. Assembly of disk colloids, or closely related oblate ellipsoids, in AC electric fields has not been previously studied. However, disk particles have the same cross sectional shape as spheres, which allows their microstructures to be compared with electric field mediated assembly of quasi-2D spherical colloids.²⁷⁻²⁹ When hard disks are concentrated above an effective area fraction ~ 0.7 , crystalline states of increasing density are obtained, and lower area fractions produce amorphous fluid states of varying density (hard disks also have intermediate hexatic state but only in large system sizes).^{7,41} Although dipolar interactions could alter the fluid-solid transition compared to hard disks, results in **Fig. 2** show the average area fraction and local 6-fold order are consistent with hard disk behavior. Results in **Fig. 2** demonstrate the average area particle area fraction ($\langle\eta\rangle$) and hexagonal order ($\langle C_6\rangle$) can be designed by choosing the correct field amplitude.

Simulation results in agreement with experiments for electric field mediated disk assembly (**Fig. 2**) help understand the balance of dipolar interactions and particle packing effects that yield the resulting microstructures. Simulation results were obtained using electrostatic and dipolar interactions that previously worked for AC electric field mediated assembly of spherical colloids between parallel electrodes.²⁷⁻²⁹ Although more rigorous potentials could be used to compute dipolar interactions between disk particles,^{22,23} the qualitative and quantitative agreement of the simulations and experiments in **Fig. 2** (*i.e.*, $\langle\eta\rangle$, $\langle C_6\rangle$) demonstrate circular disk shaped particles indeed behave similar to quasi-2D spherical colloids in AC electric fields. These results show that dipole-field interactions compress particles into dense fluid and crystal states without forming dipolar chains as in electrorheological fluids. This indicates dipole-dipole and dipole-field interactions required to orient particles into chains in the field direction are dominated by dipole interactions with non-uniform shaped fields that concentrate particles at the electrode center. As a result, the assembled microstructures correspond to essentially hard disk states without obvious effects of dipolar interactions beyond their role in concentrating particles. This also provides a reference case as we explore additional shapes in the following.

Elliptical Prisms

With an understanding of AC field mediated colloidal disk assembly, we next investigate elliptical prism particle assembly. Elliptical prisms were chosen to stretch disks along a single axis to systematically investigate how anisotropy changes assembled microstructures. Experimental

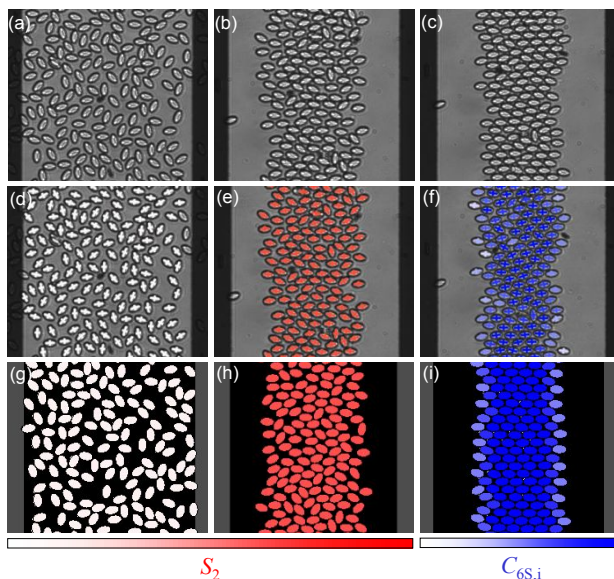


Fig. 3. Elliptical prisms with $r_x = 4.1 \mu\text{m}$ and $r_y = 2.3 \mu\text{m}$ ($r_x/r_y=1.8$) in varying density liquid, liquid crystalline, and crystalline states. Experiments without (a-c) and with (d-f) order parameter coloring and simulations (g-i) show assembled states as a function of average area fraction ($\langle\eta\rangle$), applied electric field amplitude (E_0), and average local nematic order (S_2 , Eq. (2)) or 6-fold order via “stretched” local 6-fold connectivity ($C_{6S,i}$, Eq. (5)). Particles are individually colored by S_2 from 0-1 (white-red scale) or $C_{6S,i}$ from 0-1 (white-blue scale). Images and renderings show (left-to-right, “e” and “s” subscripts refer to experimental and simulated values) moderate density liquid ($\langle\eta\rangle=0.45$, $E_0=0.2\text{V/mm}$, $S_{2,e}=0.06\pm 0.03$, $S_{2,s}=0.07\pm 0.03$), nematic liquid crystal state ($\langle\eta\rangle=0.67$, $E_0=6\text{V/mm}$, $S_{2,e}=0.74\pm 0.03$, $S_{2,s}=0.71\pm 0.03$), and crystalline state ($\langle\eta\rangle=0.86$, $E_0=20\text{V/mm}$, $\langle C_{6S}\rangle_e=0.77\pm 0.23$, $\langle C_{6S}\rangle_s=0.86\pm 0.00$). The AC electric field frequency in all cases is 5MHz

assembly of elliptical prisms ($r_x/r_y=1.8$) was measured vs. field strength and concentration (**Fig. 3**). As with disks, results show increasing area fractions at the electrode gap center with increasing field strengths, but now with orientational order in the field direction and three distinct microstructures. At low fields, the average area fraction is low, and a concentrated liquid state is observed with no orientational or positional order (**Fig. 3** left). At intermediate fields, particles concentrate and align into nematic states, where a nematic order parameter (S_2)^{7,30} quantifies orientational order along a director in the field direction (**Fig. 3** middle). At the highest field strengths, elliptical particles crystallize with high orientational and positional order characterized by high stretched 6-fold symmetry ($\langle\langle C_{6S} \rangle\rangle$) (**Fig. 3** right). These results show clearly the ability to assemble quasi-2D liquid, nematic, and crystal states of elliptical prisms in electric fields.

Simulation results help identify how shape anisotropy influences both dipolar interactions and packing effects and their balance in determining the observed microstructures. It is important to note that point dipole potentials do not quantitatively (and in some a, qualitatively) capture the microstructures in **Fig. 3**. Instead, we use an ellipsoidal dipole,⁴² which we have shown can be mimicked by a novel stretched point dipole;²⁴ in this work, both potentials quantitatively capture the three liquid, nematic, and crystal microstructures, and their transition conditions in terms of applied field and average concentration (area fraction). We also note that the field produces a nematic phase that is unexpected for hard ellipses with $r_x/r_y=1.8$, where normally $r_x/r_y < 1.6$ produces plastic crystal states and $r_x/r_y > 2.4$ is required to form nematic states.^{8,31} Dipolar alignment with the external field creates a nematic state that it is not expected from packing hard particles of the same shape. However, in contrast, in the crystal state, hard particle packing produces a close packed crystal with stretched hexagonal symmetry, whereas dipolar interactions alone are known to yield more open lattice structures (via dipolar angular contact minima that produce more open packings).^{20,43} The results demonstrate the delicate balance of packing effects and dipolar interactions, which both depend on particle shape, and produce nematic and crystal states that are unexpected without considering detailed models of both contributions. In short, dominant dipolar interactions yield an unexpected nematic state, and then in a reversal, dominant packing effects produce a close packed crystal state.

Square Prisms

In addition to stretching disks into ellipses to influence orientational order, the role of adding corners without stretching is considered by investigating square particles (**Fig. 4**). Corners significantly affect how particles orient relative to each other to produce 4-fold order in liquid crystal and crystal states and enable packing up to area fractions approaching unity. We quantify orientational order using a global tetratic order parameter, T_4 , which varies from 0 for liquids to 1 for square crystals; values of ~ 0.5 indicate tetratic states without positional order but with orientational order aligned with a global bidirector (alignment along two directions). We quantify positional order of squares in crystal states with a metric for 4-fold order ($\langle\langle C_4 \rangle\rangle$, the average number of connected neighbor particles with 4-fold bond orientational order).

The lowest field yields liquid states with no orientational or positional order (**Fig. 4** left). At intermediate fields, significant tetratic order is observed with sensitivity to several factors (**Fig. 4** middle). Tetratic order is enhanced in simulations compared to experiments, when both are at the same field conditions and average area fractions, which suggests particle imperfections, may have a role in the degree of tetratic order. Practically, finite size polydispersity and shape nonuniformity may be important to how tetratic order is influenced by nearly square corners. Our simulations include small rounding of the hard particle corners (see *Methods*),^{7,10} which can

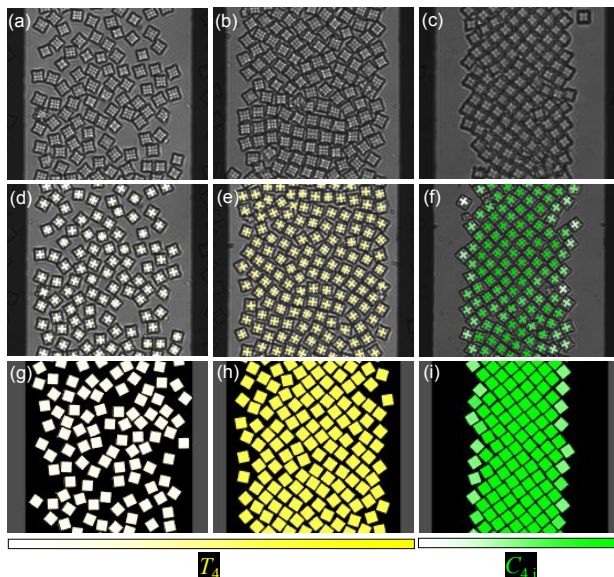


Fig. 4. Square prisms with $r_x = r_y = 3.9 \mu\text{m}$ in varying density liquid, liquid crystalline, and crystalline states. Experiments without (a-c) and with (d-f) order parameter coloring and simulations (g-i) show assembled states as a function of average area fraction ($\langle\eta\rangle$), applied electric field amplitude (E_0), and average local tetratic order (T_4 , Eq. (3)) or local 4-fold connectivity ($C_{4,i}$, Eq. (5)). Particles are individually colored by T_4 from 0-1 (white-yellow scale) or $C_{4,i}$ from 0-1 (white-green scale). Images and renderings show (left-to-right, “e” and “s” subscripts refer to experimental and simulated values) moderate density liquid ($\langle\eta\rangle=0.54$, $E_0=1\text{V/mm}$, $T_{4,e}=0.09\pm 0.06$, $T_{4,s}=0.09\pm 0.04$), nearly tetratic liquid crystal state ($\langle\eta\rangle=0.74$, $E_0=3\text{V/mm}$, $T_{4,e}=0.22\pm 0.06$, $T_{4,s}=0.69\pm 0.04$), and crystalline state ($\langle\eta\rangle=0.8$, $E_0=20\text{V/mm}$, $\langle C_4\rangle_e=0.83\pm 0.26$, $\langle C_4\rangle_s=0.87\pm 0.05$). The AC electric field frequency in all cases is 5MHz

account for the limited resolution of the lithographically fabricated particles, but may also not capture the effect of electrostatic interactions at corners with high curvature. In other words, additional effective rounding of corners by soft repulsion could also reduce tetratic order at intermediate concentrations/fields. Despite the differences in the degree of tetratic order, the area fractions when tetratic order is maximized between fluid and crystal states falls within the expected range for hard squares.^{7,9,10} Similar to hard disks, the assembled microstructures correspond to essentially hard square states without obvious effects of dipolar interactions beyond their role in concentrating particles at the electric field minimum in the electrode center.

The square prism particles are compressed into crystals (**Fig. 4** right) at the expected area fraction and degree of 4-fold order expected for hard squares.^{7,9,10} The crystal microstructure is a basic square packing consistent with hard square results, without evidence of rhombic,⁴⁴ Λ_1 -lattice packing,⁴⁵ or chains⁴⁶ observed with dipolar and/or depletion interactions. This observation is consistent with compression in fields dominating dipolar interactions that do not obviously influence the closed packed states similar to disks and ellipses. Another notable feature of the crystal structure is the ~ 45 -degree tilted orientation of resulting square lattice relative to the field direction. We have measured the energy landscape of single square prisms in the same electric field geometry, and they have no orientational dependence, which also suggests this configuration is due to packing effects. This orientation has been reported for 2D confinement of hard squares in slit confinement when the wall spacing is incommensurate with fitting an integer number of lattice layers normal to the walls.⁴⁷ Soft confinement by the nonuniform AC electric field shape appears to favor the titled orientation like frustrated confinement between hard walls.

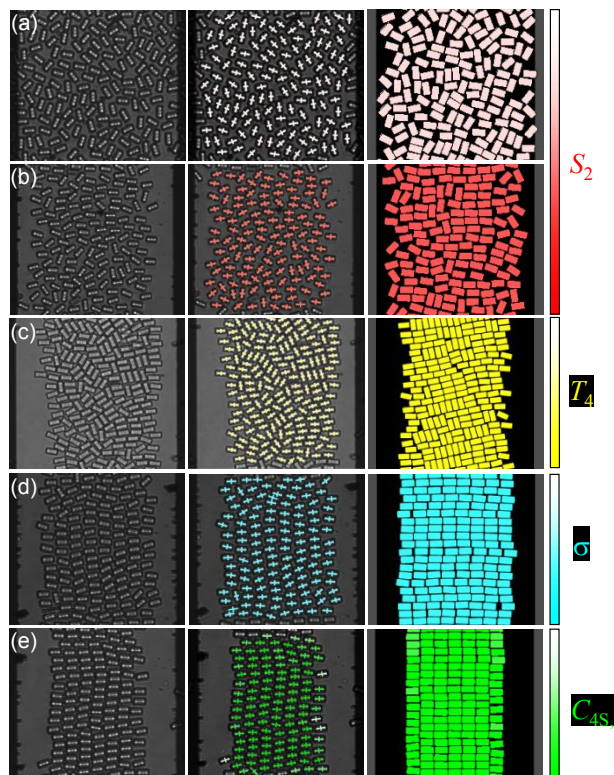


Fig. 5. Rectangular prisms with $r_x = 4.1 \mu\text{m}$ and $r_y = 2.3 \mu\text{m}$ ($r_x/r_y=1.8$) in varying density liquid, liquid crystalline, and crystalline states. Experiments without (left) and with (center) order parameter coloring and simulations (right) show assembled states as a function of average area fraction ($\langle\eta\rangle$), applied electric field amplitude (E_0), and nematic order (S_2 , red, Eq. (2)), tetratic order (T_4 , yellow, Eq. (3)), smectic order (σ , cyan, Eq. (4)), and “stretched” local 4-fold connectivity ($C_{4S,i}$, green, Eq. (5)). Images and renderings show (top-to-bottom, “e” and “s” subscripts refer to experimental and simulated values): (a) moderate density liquid ($\langle\eta\rangle=0.63$, $E_0=0.2\text{V/mm}$, $S_{2,e}=0.07\pm0.04$, $S_{2,s}=0.06\pm0.03$), (b) nematic liquid crystal ($\langle\eta\rangle=0.78$, $E_0=2.1\text{V/mm}$, $S_{2,e}=0.57\pm0.04$, $S_{2,s}=0.72\pm0.05$), (c) tetratic liquid crystal ($\langle\eta\rangle=0.75$, $E_0=20.6\text{V/mm}$, $T_{4,e}=0.25\pm0.06$, $T_{4,s}=0.93\pm0.02$), (d) smectic liquid crystal ($\langle\eta\rangle=0.5-0.6$, $E_0=5.2\text{V/mm}$, $\sigma_e=0.47\pm0.06$, $\sigma_s=0.58\pm0.11$), and (e) crystal with stretched 4-fold order ($\langle\eta\rangle=0.93$, $E_0=12.4\text{V/mm}$, $\langle C_{4S}\rangle_e=0.90\pm0.19$, $\langle C_{4S}\rangle_s=0.96\pm0.00$). The AC electric field frequency in all cases is 5MHz.

Rectangular Prisms

The last shape we investigate in detail is a rectangular prism, which is anisotropic like ellipses and has corners like squares. Experiments and simulations of rectangular prisms in AC electric fields show five distinct microstructures (**Fig. 5**). At infinite dilution, single rectangular prisms can be aligned with the field in 6 possible orientations by tuning electric field frequency.^{22,23} At 5MHz, the rectangles’ major axes align with the field direction with their largest flat face orients parallel to the substrate, which is similar to elliptical prisms. Particles sample different orientations via thermal fluctuations with the range of orientations determined by the field amplitude, which determines the degree to which particles align before compression into condensed microstructures. As a result, many of the structures discussed in the following are metastable states determined by field-mediated alignment prior to initiating field-mediated compression.

To check liquid and liquid crystal states for alignment along a director or bidirector, we quantify microstructures using nematic, S_2 , and tetratic, T_4 , order parameters. A nearly isotropic

liquid state with weak nematic (and tetratic) order is observed at low field strengths that barely confine particles within the electrodes (**Fig. 5a**). Increasing the field to align and concentrate particles produces a nematic state (**Fig. 5b**). While nematic states are expected for rectangles with the aspect ratio in this work ($r_x/r_y=1.8$),^{7,33} the nematic found in this work forms at lower than expected concentrations due to dipolar alignment with the field direction. In contrast, a kinetically trapped tetratic liquid crystal state (**Fig. 5c**) is achieved by a sudden quench from the disordered fluid state, which causes particles to become aligned in two orthogonal directions. Hard rectangles of the same aspect ratio form equilibrium tetratic phases at lower concentrations in much larger system sizes,^{7,33} however, the small system size and clear pathway dependence suggests the tetratic state here is a kinetically trapped state. The difference between the experimental and simulated tetratic order parameters also shows a sensitivity of the resulting state to the kinetic pathway.

Smectic liquid crystal states are characterized by an order parameter, σ , that quantifies positional order in the direction of orientational order (along the director), while particles remain fluid orthogonal to the director. High σ values indicate 2D smectic states (**Fig. 5d**) occur when nematics are compressed into 8 liquid layers with one-dimensional positional order between the electrodes. Layers in experiments clearly remain liquid without positional order perpendicular to the field direction, but with positional order via layering parallel to the field direction. This indicates dipolar interactions allow particles to remain mobile within layers. Particles are less fluid in simulations due to system size effects (*i.e.*, small simulation box with periodic boundaries). Smectic states have been observed for simulated 2D hard rod confinement,⁴⁸ and in 3D sedimented spherocylinders in electric fields,⁴⁹ but we are not aware of prior observations of 2D smectic states in AC electric fields. The experimental smectic state has a slight tilt to particles within layers, similar to a smectic C phase,⁴⁸ but this feature is relatively minor. The tilt likely results from a balance of field mediated compression and particle alignment, which does not appear to be well captured by the subtle balance of dipolar potentials in the simulation (**Fig. 5d**). The rectangular prism particle crystal state (**Fig. 5e**) has four-fold symmetry like squares but stretched along the particle long axis in alignment with the field. While aspect ratio determines preferred liquid crystal states, corners more significantly influences the crystal symmetry.⁷

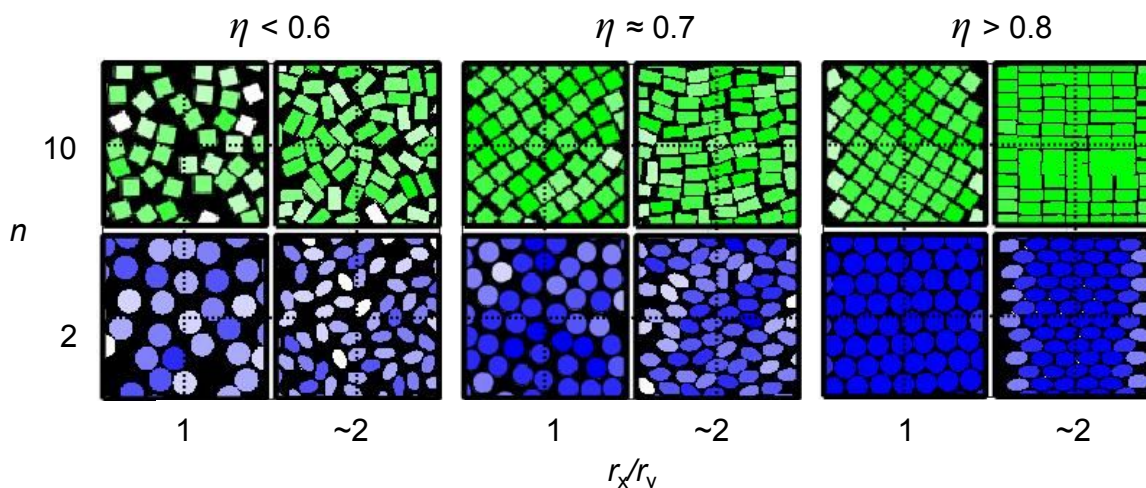


Fig. 6. State diagram of particle shape dependent microstructures assembled in AC electric fields. Images show representative simulation renderings vs. particle aspect ratio (r_x/r_y), superellipse corner parameter (n), and area fraction (η). Particles are colored by local six-fold order (C_6 , blue) for $n \approx 2$ and local four-fold order (C_4 , green) for $n = 10$.

State Diagram: Particle Shape Dependent Microstructures

We summarize how particle shape and dipolar interactions together determine 2D liquid crystalline and crystalline microstructures in AC electric fields (**Fig. 6**). We show representative states as a function of particle aspect ratio (r_x/r_y), superellipse corner parameter (n), and area fraction (η). This summary clearly shows the effects of particle anisotropy and corners in determining available microstructural states for monolayers of superelliptical prisms with dipolar interactions. Because particle materials and field shape are constant, shape anisotropy and curvature are the dominant effect determining the resulting microstructures. Particle concentration within the nonuniform electric fields is determined by the applied field strength, particle number, electrode dimensions, and particle volume, so area fraction is used for consistency across all shapes and conditions and for comparison with hard particle phase behavior.²⁴

Overall, the absence of corners produces six-fold order in crystalline states, whereas the presence of corners produces four-fold order in crystalline states. Likewise, anisotropy tends to produce nematic liquid crystal states, which form at lower-than-expected area fractions for particles based on dipolar alignment with the field. In contrast, isotropic particle shapes produce no obvious intermediate states between liquid and crystal states, such as hexatic or tetratic states, which are only expected at exceptionally large system sizes for hard particles.⁹ Anisotropy and corners together in rectangular prism particles produce additional tetratic and smectic liquid crystals states, which result from packing, alignment with the field, and corners that inhibit rotation within assembled structures. The ability of the field to concentrate and align particles, together with shape dependent packing effects, reliably and reproducibly yields a variety of well-defined liquid, liquid crystalline, and crystalline microstructures for use in particle-based surface materials and devices.

Conclusions

Our microscopy and computer simulation results demonstrate the microstructural diversity from AC electric field mediated assembly of superelliptical prism particles, which include liquid, liquid crystalline, and crystalline states. Our results based on microstructural characterization with order parameters show how systematically varying particle anisotropy and corner curvature (for disks, ellipses, squares, and rectangles) introduces nematic, tetratic, and smectic liquid crystal states and determines whether crystalline states have four- or six- fold symmetry. Practically, we demonstrate kinetically viable routes to assemble different particle shapes, with varying aspect ratio and corner curvature, into target liquid crystal and crystalline microstructures. Our results show the ability to achieve all microstructures possible in corresponding hard particle phases, but also show how dipolar interactions produce microstructures at different conditions as well as additional microstructures not possible in hard particle systems.

In general, increasing aspect ratio favors nematic states, adding corners favors tetratic states, and higher aspect ratios together with corners can yield smectic states. Dipole-field interactions produce particle alignment with the field and nematic states at lower concentrations and aspect ratios than what is expected from hard particle phase behavior. In the high concentration limit approaching closed packed crystalline states, the dipole-field interaction compresses particles into crystal states dominated by hard particle packing effects without obvious dipolar chaining due to dipole-dipole interactions. Crystal structures are determined by particle shape, where corners (*i.e.*, squares, rectangles) favor four-fold order and the absence of corners (*i.e.*, disks, ellipses) favor six-fold order. By systematically exploring how particle anisotropy and curvature

determine a variety of assembled microstructures in electric fields, our results provide design rules for particle shapes required to fabricate desired particle-based surface materials and devices.

Ongoing and future work could extend the approaches reported in this work into scalable technologies using electrode arrays for printing particles (e.g., Xerography, nanoparticle printing⁵⁰). In addition, understanding the dynamics of microstructure assembly and disassembly processes could enable feedback control over particle reconfigurability in displays (e.g., liquid crystal displays,⁵¹ particle displays⁵²) and in tunable devices (e.g., antennas,^{53,54} metasurfaces^{4,6}).

Acknowledgments

We acknowledge financial support by the National Science Foundation CBET 2113594.

References

1. Wu, N., D. Lee, and A. Striolo, *Anisotropic Particle Assemblies*. Vol. 1. 2018: Elsevier. 366.
2. McDougal, A., B. Miller, M. Singh, and M. Kolle, *Biological growth and synthetic fabrication of structurally colored materials*. Journal of Optics, 2019. **21**(7): p. 073001.
3. Sanchez, C., H. Arribart, and M.M. Giraud Guille, *Biomimeticism and bioinspiration as tools for the design of innovative materials and systems*. Nature Materials, 2005. **4**: p. 277.
4. Ni, X., Z.J. Wong, M. Mrejen, Y. Wang, and X. Zhang, *An ultrathin invisibility skin cloak for visible light*. Science, 2015. **349**(6254): p. 1310-1314.
5. Chen, S., Z. Li, Y. Zhang, H. Cheng, and J. Tian, *Phase Manipulation of Electromagnetic Waves with Metasurfaces and Its Applications in Nanophotonics*. Advanced Optical Materials, 2018. **6**(13): p. 1800104.
6. Zheludev, N.I. and Y.S. Kivshar, *From Metamaterials to Metadevices*. Nat. Mater., 2012. **11**(11): p. 917-924.
7. Torres-Díaz, I., R.S. Hendley, A. Mishra, A.J. Yeh, and M.A. Bevan, *Hard superellipse phases: particle shape anisotropy & curvature*. Soft Matter, 2022.
8. Bautista-Carbajal, G. and G. Odriozola, *Phase diagram of two-dimensional hard ellipses*. The Journal of Chemical Physics, 2014. **140**(20): p. 204502.
9. Anderson, J.A., J. Antonaglia, J.A. Millan, M. Engel, and S.C. Glotzer, *Shape and Symmetry Determine Two-Dimensional Melting Transitions of Hard Regular Polygons*. Physical Review X, 2017. **7**(2).
10. Avendaño, C. and F.A. Escobedo, *Phase behavior of rounded hard-squares*. Soft Matter, 2012. **8**(17): p. 4675.
11. Wu, N., D. Lee, and A. Striolo, *Anisotropic Particle Assemblies*. 2018, Amsterdam: Elsevier.
12. Glotzer, S.C. and M.J. Solomon, *Anisotropy of building blocks and their assembly into complex structures*. Nat Mater, 2007. **6**(7): p. 557-562.
13. Damasceno, P.F., M. Engel, and S.C. Glotzer, *Predictive Self-Assembly of Polyhedra into Complex Structures*. Science, 2012. **337**(6093): p. 453-457.
14. Zheng, Z., R. Ni, Y. Wang, and Y. Han, *Translational and rotational critical-like behaviors in the glass transition of colloidal ellipsoid monolayers*. Science Advances, 2021. **7**(3): p. eabd1958.
15. Liu, X., H. Wang, Z. Zhang, J.M. Kosterlitz, and X.S. Ling, *Nature of the glass transition in 2D colloidal suspensions of short rods*. New Journal of Physics, 2020. **22**(10): p. 103066.
16. Shah, A.A., H. Kang, K.L. Kohlstedt, K.H. Ahn, S.C. Glotzer, C.W. Monroe, and M.J. Solomon, *Liquid Crystal Order in Colloidal Suspensions of Spheroidal Particles by Direct Current Electric Field Assembly*. Small, 2012. **8**(10): p. 1551-1562.

17. Kuijk, A., T. Troppenz, L. Fillion, A. Imhof, R. van Roij, M. Dijkstra, and A. van Blaaderen, *Effect of external electric fields on the phase behavior of colloidal silica rods*. *Soft Matter*, 2014. **10**(33): p. 6249-6255.
18. Liu, B., T.H. Besseling, M. Hermes, A.F. Demirors, A. Imhof, and A. van Blaaderen, *Switching plastic crystals of colloidal rods with electric fields*. *Nat Commun*, 2014. **5**: p. 3092.
19. Panczyk, M.M., J.-G. Park, N.J. Wagner, and E.M. Furst, *Two-Dimensional Directed Assembly of Dicolloids*. *Langmuir*, 2013. **29**(1): p. 75-81.
20. Singh, J.P., P.P. Lele, F. Nettesheim, N.J. Wagner, and E.M. Furst, *One- and two-dimensional assembly of colloidal ellipsoids in ac electric fields*. *Physical Review E*, 2009. **79**(5): p. 050401.
21. Boehm, S.J., L. Lin, K. Guzman Betancourt, R. Emery, J.S. Mayer, T.S. Mayer, and C.D. Keating, *Formation and frequency response of two-dimensional nanowire lattices in an applied electric field*. *Langmuir*, 2015. **31**(21): p. 5779-86.
22. Rupp, B., I. Torres-Diaz, X. Hua, and M.A. Bevan, *Measurement of Anisotropic Particle Interactions with Nonuniform ac Electric Fields*. *Langmuir*, 2018. **34**(7): p. 2497-2504.
23. Torres-Díaz, I., B. Rupp, Y. Yang, and M.A. Bevan, *Energy landscapes for ellipsoids in non-uniform AC electric fields*. *Soft Matter*, 2018. **14**(6): p. 934-944.
24. Hendley, R.S., I. Torres-Díaz, and M.A. Bevan, *Anisotropic colloidal interactions & assembly in AC electric fields*. *Soft Matter*, 2021. **17**(40): p. 9066-9077.
25. Hernandez, C.J. and T.G. Mason, *Colloidal Alphabet Soup: Monodisperse Dispersions of Shape-Designed LithoParticles*. *The Journal of Physical Chemistry C*, 2007. **111**(12): p. 4477-4480.
26. Edwards, T.D. and M.A. Bevan, *Controlling Colloidal Particles with Electric Fields*. *Langmuir*, 2014. **30**(36): p. 10793-10803.
27. Juarez, J.J. and M.A. Bevan, *Interactions and Microstructures in Electric Field Mediated Colloidal Assembly*. *J. Chem. Phys.*, 2009. **131**: p. 134704.
28. Juarez, J.J., J.-Q. Cui, B.G. Liu, and M.A. Bevan, *kT-Scale Colloidal Interactions in High Frequency Inhomogeneous AC Electric Fields. I. Single Particles*. *Langmuir*, 2011. **27**(15): p. 9211-9218.
29. Juarez, J.J., B.G. Liu, J.-Q. Cui, and M.A. Bevan, *kT-Scale Colloidal Interactions in High-Frequency Inhomogeneous AC Electric Fields. II. Concentrated Ensembles*. *Langmuir*, 2011. **27**(15): p. 9219-9226.
30. Frenkel, D. and R. Eppenga, *Evidence for algebraic orientational order in a two-dimensional hard-core nematic*. *Phys Rev A Gen Phys*, 1985. **31**(3): p. 1776-1787.
31. Cuesta, J.A. and D. Frenkel, *Monte Carlo simulation of two-dimensional hard ellipses*. *Phys Rev A*, 1990. **42**(4): p. 2126-2136.
32. Wojciechowski, K.W. and D. Frenkel, *Tetratic Phase In the Planar Hard Square System?* *J. Comput. Methods Sci. Eng.*, 2004. **10**: p. 235.
33. Donev, A., J. Burton, F.H. Stillinger, and S. Torquato, *Tetratic order in the phase behavior of a hard-rectangle system*. *Physical Review B*, 2006. **73**(5).
34. Varga, S., P. Gurin, J.C. Armas-Pérez, and J. Quintana-H, *Nematic and smectic ordering in a system of two-dimensional hard zigzag particles*. *The Journal of Chemical Physics*, 2009. **131**(18): p. 184901.
35. ten Wolde, P.R., M.J. Ruiz-Montero, and D. Frenkel, *Numerical Calculation of the Rate of Crystal Nucleation in a Lennard-Jones System at Moderate Undercooling*. *J. Chem. Phys.*, 1996. **104**: p. 9932.

36. Bitter, J.L., Y. Yang, G. Duncan, H. Fairbrother, and M.A. Bevan, *Interfacial and Confined Colloidal Rod Diffusion*. Langmuir, 2017. **33**(36): p. 9034-9042.
37. Juarez, J.J., S.E. Feicht, and M.A. Bevan, *Electric Field Mediated Assembly of Three Dimensional Equilibrium Colloidal Crystals*. Soft Matter, 2012. **8**(1): p. 94-103.
38. Edwards, T.D., D.J. Beltran-Villegas, and M.A. Bevan, *Size Dependent Thermodynamics and Kinetics in Electric Field Mediated Colloidal Crystal Assembly*. Soft Matter, 2013. **9**(38): p. 9208-9218.
39. Zhang, J., Y. Zhang, and M.A. Bevan, *Spatially Varying Colloidal Phase Behavior on Multi-Dimensional Energy Landscapes*. J. Chem. Phys., 2020. **152**: p. 054905.
40. Zheng, Z., R. Ni, F. Wang, M. Dijkstra, Y. Wang, and Y. Han, *Structural signatures of dynamic heterogeneities in monolayers of colloidal ellipsoids*. Nature Communications, 2014. **5**: p. 3829.
41. Engel, M., J.A. Anderson, S.C. Glotzer, M. Isobe, E.P. Bernard, and W. Krauth, *Hard-disk equation of state: First-order liquid-hexatic transition in two dimensions with three simulation methods*. Physical Review E, 2013. **87**(4): p. 042134.
42. Stratton, J.A., *Electromagnetic Theory*. 1941, New York: McGraw-Hill Book Company, Inc. 615.
43. Tao, R. and J.M. Sun, *Three-dimensional structure of induced electrorheological solid*. Phys. Rev. Lett., 1991. **67**(3): p. 398.
44. Zhao, K., R. Bruinsma, and T.G. Mason, *Entropic crystal-crystal transitions of Brownian squares*. Proc Natl Acad Sci U S A, 2011. **108**(7): p. 2684-7.
45. Jiao, Y., F.H. Stillinger, and S. Torquato, *Optimal packings of superdisks and the role of symmetry*. Phys Rev Lett, 2008. **100**(24): p. 245504.
46. Vutukuri, H.R., F. Smalenburg, S. Badaire, A. Imhof, M. Dijkstra, and A. van Blaaderen, *An experimental and simulation study on the self-assembly of colloidal cubes in external electric fields*. Soft Matter, 2014. **10**(45): p. 9110-9.
47. Bautista-Carbajal, G., P. Gurin, S. Varga, and G. Odriozola, *Phase diagram of hard squares in slit confinement*. Sci Rep, 2018. **8**(1): p. 8886.
48. Geigenfeind, T., S. Rosenzweig, M. Schmidt, and D. de Las Heras, *Confinement of two-dimensional rods in slit pores and square cavities*. J Chem Phys, 2015. **142**(17): p. 174701.
49. Kuijk, A., T. Troppenz, L. Fillion, A. Imhof, R. van Roij, M. Dijkstra, and A. van Blaaderen, *Effect of external electric fields on the phase behavior of colloidal silica rods*. Soft Matter, 2014. **10**(33): p. 6249-55.
50. Kraus, T., L. Malaquin, H. Schmid, W. Riess, N.D. Spencer, and H. Wolf, *Nanoparticle printing with single-particle resolution*. Nature Nanotechnology, 2007. **2**(9): p. 570-576.
51. Chen, H.-W., J.-H. Lee, B.-Y. Lin, S. Chen, and S.-T. Wu, *Liquid crystal display and organic light-emitting diode display: present status and future perspectives*. Light: Science & Applications, 2018. **7**: p. 17168.
52. Comiskey, B., J.D. Albert, H. Yoshizawa, and J. Jacobson, *An electrophoretic ink for all-printed reflective electronic displays*. Nature, 1998. **394**: p. 253-255.
53. Bahukudumbi, P., W.N. Everett, A. Beskok, G.H. Huff, D. Lagoudas, Z. Ounaies, and M.A. Bevan, *Colloidal Microstructures, Transport, and Impedance Properties within Interfacial Microelectrodes*. Appl. Phys. Lett., 2007. **90**: p. 224102.
54. Long, S.A., W.M. Dorsey, G.H. Huff, N. Brennan, B. Rupp, and M.A. Bevan, *Fluidic-Enabled Reconfigurable Patch With Integrated Dielectric Spectrometer*. Antennas and Wireless Propagation Letters, IEEE, 2014. **13**: p. 1116-1119.